A NEW UNDERSTANDING OF DAMAGE MECHANISM OF CAI

Y. Yang*, S. Li

Faculty of Engineering, University of Nottingham, Nottingham NG7 2RD, UK
** Corresponding author (emxyy2@nottingham.ac.uk)*

Keywords: impact, delamination, compression, CAI

Abstract
The investigation of damage mechanism of compression after impact (CAI) using finite element method improves the prediction method of residual compressive strength of impacted laminate. The numerical model proposed in this paper simulates two damage modes simultaneously: laminar in-plane failure and interfacial delamination propagation. The results obtained show that, when the laminate bears multi-delamination resulting from low-speed impact, the dominant damage mechanism of CAI is in-plane failure. The implication is that it would be reasonable to predict residual compressive strength of impacted laminate by only considering the in-plane failure modes.

1. Introduction

It is well known that composite laminate is susceptible to foreign object impact, usually classified as low-velocity impact, which could result in 60% compressive strength loss without obvious surface damage. Therefore in aviation industry, a large number of CAI tests have to be conducted to determine the allowable design values. For the purpose of cost reduction and reliability improvement, prediction method of CAI has always been an interesting topic in the realm of advanced composite laminates. However, so far, there are mainly two different viewpoints, which lead two completely different prediction methods.

The common viewpoint of CAI is that the delaminated area buckles when the impact-damaged laminate is subjected to in-plane compression, and sublaminates in this area have a tendency of relative movements which may result in rising stress levels around delamination crack tips. With the increasing compressive load, the delamination propagation can be triggered when the energy release rate (ERR) at the crack tip exceeds its threshold. The whole laminate could collapse because of unstable delamination propagation. Based on this viewpoint, many researchers contributed huge amount of work in the past three decades [1] focusing mainly on delamination propagation problems, from one-dimensional delamination [2] to two dimensional delamination [3], from single delamination to multi-delamination [4-9], from regular shaped delamination (circular or elliptical) to double spiral fan-shaped delamination [10]. However, computation cost rockets with the increasing complexity of this delamination model, which needs to incorporate delamination propagation, geometric nonlinearity, structural instability and contact of multiple interfaces simultaneously [11-13].

The other viewpoint considers the failure of CAI as a consequence of stress concentration [14-15]. Since delaminated area can only sustain reduced compressive load when it buckles due to in-plane compression, stress redistributes and stress concentration arises around the edge of delaminated area, which leads catastrophic failure of the whole plate when the concentrated stress exceeds its strength. Therefore, the stiffness of the delaminated area is deducted to simulate the less load-sustainability effect, and computation cost is relatively low because only in-plane failure mode is considered in this model [16-17].

The reason why two different viewpoints co-exist for decades is the lack of solid experimental evidence. The transient catastrophic failing process impedes any further valuable phenomenon to be captured.

Therefore, in this paper, numerical simulation is implemented to explore the damage mechanism of CAI. It would provide useful suggestion for appropriate selection of prediction method of CAI.

2. Analysis model

2.1 Lamina and laminate

The unidirectional lamina which constitutes the laminate in this paper is IM7/8551-7 [18], of which the typical data for the properties is listed in Table 1.

Fiber type	IM7
Matrix	8551-7
Longitudinal modulus E1 (GPa)	165
Transverse modulus E2 (GPa)	8.4
In-plane shear modules G12 (GPa)	5.6
Major Poisson's ratio v12	0.34
Longitudinal tensile strength xt (MPa)	2560
Longitudinal compressive strength xc (MPa)	1590
Transverse tensile strength yt (MPa)	73
Transverse compressive strength yc (MPa)	185
In-plane shear strength s12 (MPa)	90
Thickness (mm)	0.1425
Mode I energy release rate GIc (J/m2)	200
Mode II energy release rate GIIc (J/m2)	610

Table 1. Mechanical properties for the unidirectional lamina of IM7/8551-7

The layup sequence of the numerical model here is $[45/0/-45/90]_{3S}$, in which the 0 degree lamina aligns with length direction of the model, which is the compression-loading direction as well.

2.2 Numerical model

Finite element method is employed here to investigate the damage mechanism using software ABAQUS as the analysing tool. The whole laminate is discretised into (n+1) sublaminates in thickness direction according to the prescribed delamination number n. Each sublaminate, containing a number of laminae, is simulated as a layer of continuous shell elements. For each delamination, contact condition between the two neighbouring sublaminates is introduced to prevent interpenetration when the sublaminates deform. For the rest of the area on the same

interface, a layer of cohesive elements is inserted between these two sublaminates to allow potential delamination propagation.

One of the prevalent test standards of CAI is ASTM D7137 [19], on which the principles of the numerical model presented in this paper is based (Fig. 1). The in-plane dimensions of the model are 150mm in length and 100mm in width. For boundary conditions on both loading edges, the magnitude of the displacement in the direction of compression is prescribed, and the out-of-plane deflection is constrained while allowing the edge to displace freely in the tangential in-plane direction. According to ASTM D7137, in order to prevent global buckling, two pairs of slide plates with knife edges are used in the test rig, one on each side along the length direction of the specimen, approximately 4mm from the edge. In the numerical model, the nodes falling onto these two lines are constrained from out-of-plane deflections.

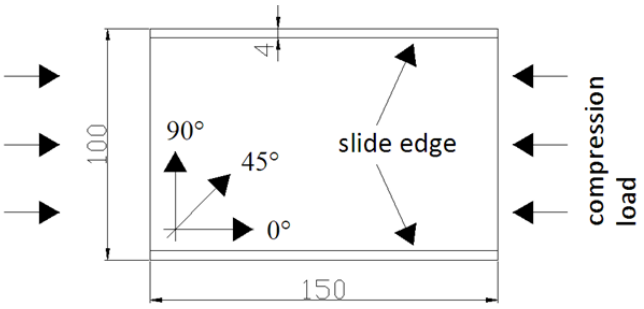

Figure 1. Plane view of the numerical model

As the main task here is to identify the dominant damage mechanism, two possible damage modes, the in-plane failure and delamination propagation are taken into consideration simultaneously in this model. The ABAQUS built-in Hashin failure criterion is introduced to simulate in-plane failure and cohesive element mentioned above for delamination propagation simulation.

Besides, in order to reduce the finite element model size, a rotational symmetric condition is employed so that only half of the laminate is constructed [20]. The scheme of the finite element model is presented in Figure 2.

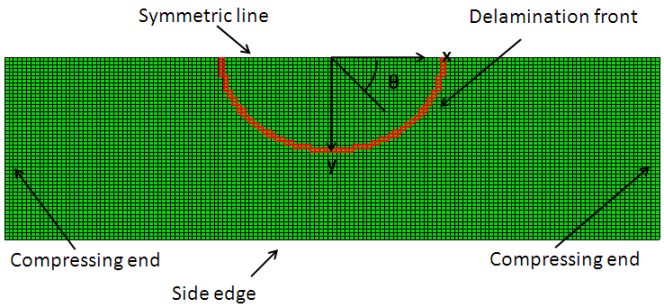

Figure. 2 Scheme of the symmetric finite element model

2.3 Parametric study matrix

Four typical cases with diverse delamination locations and distribution shape in thickness direction are analyzed. The model references and corresponding brief descriptions are listed in Table 2.

Case 1

Assume that there is only one circular delamination of 25mm radius in the laminate. It is located thickness direction at 3 different positions: between 12th and 13rd laminae, between 8th and 9th laminae and between 4th and 5th laminae.

Case 2

Introduce multiple circular delaminations with same radiuses of 25mm. These delaminations distribute evenly in thickness, but number of delaminations in each model is 3, 5, 7 or 23, respectively in these four models.

Case 3

Alter the multi-delamination distribution through the thickness from cylindrical shape in Case 2 to spindle shape, i.e. the delamination being of a radius of 5mm near one surface, gradually increasing to 25mm in the central depth before decreasing back to 5mm again near the other surface.

Case 4

Alter the spindle multi-delamination distribution in Case 3 to cone shape, i.e. the minimum delamination of a radius of 5mm close to one surface and monotonously expands to maximum 25mm close to other surface.

Case	Reference	Description
1	N_1_12_12	Unique delamination in central depth
	N_1_8_16	Unique delamination between 8th and 16th laminae
	N_1_4_20	Unique delamination between 4th and 20th laminae
2	N_3	3 identical delaminations
	N_5	5 identical delaminations
	N_7	7 identical delaminations
	N_23	23 identical delaminations
3	N_3_SP	3 delaminations in spindle-shape distribution
	N_5_SP	5 delaminations in spindle-shape distribution
	N_7_SP	7 delaminations in spindle-shape distribution
	N_23_SP	23 delaminations in spindle-shape distribution
4	N_3_CO	3 delaminations in cone-shape distribution
	N_5_CO	5 delaminations in cone-shape distribution
	N_7_CO	7 delaminations in cone-shape distribution
	N_23_CO	23 delaminations in cone-shape distribution

Table 2. Model naming and brief description

3. Discussion

3.1 Dominant damage mode

From experimental observations of the common catastrophic failure of CAI reveal that the specimens tend to break at the central line across the width where the remaining width of intact laminate from delamination front to side edge is minimum, leaving the two broken parts

inserting into each other in a broom shape. The region cross around the section at the central line is worth extraordinarily investigation for proper understanding of the damage mechanism. To illustrate the mechanism, the state of fibre compression failure and delamination propagation within the section at two selected loading stages are captured as shown in Figure 3. One is when the fibre compression failure first occurs, and the other is when the peak compression load is reached. The reason of first selection is to identify whether delamination propagation occurs prior to fibre compression failure in 0° lamina, because once fibre failure occurs, it is followed by the catastrophic failure straightaway. The reason of second selection is to identify the dominant failure mode. Only half section view is shown while the other half can be reconstructed using the rotational symmetry. Hatched areas indicate the initial delaminations. The grey parts represent the failed areas of originally intact interfaces. The black parts represent areas of fibre compression failure.

The N_1_12_12 is examined first. From the left figure of Fig. 3(a), it can be seen that fibre compression failure initially occurs at the centre of the model when there is no interface failure. From the right figure of Fig. 3(a), it is found all 0° laminae have failed when the compression load reached its maximum. This damage pattern leads to the conclusion that this laminate fails like in-plane failure of an intact laminate. This is due to relatively thick sublaminate whose high flexural stiffness does not allow it into to buckle or deform into advanced post-buckling stage, leaving little chance for delamination propagation.

In N_1_8_16, as the location of delamination is located 4 laminae away from central interface, the relatively thinner sublaminate becomes weaker to sustain the compression load. Hence, the initial fibre compression failure occurs within the thin sublaminate (the left figure of Fig. 3(b)). As the load increases, the fibre failure propagates from centre towards side edge. When compression load reaches its maximum, the 0° laminae in thin sublaminate almost completely fail. However, only slices of fibre failure in thick sublaminate occur at the locations aligned with the front of propagating delamination. Although the onset of fibre compression failure may be at different position in each 0° lamina, the fronts of failure propagation in each lamina are likely to coincide with the instance when compressive load reaches its maximum. This "trimmed front" is due to the fact that, during the failure propagation process, stress concentration occurs at the front of delamination propagation path and becomes more and more severe as the load increases. Once the concentrated stress exceeds the material's strength in other laminae, failure occurs and propagates rapidly.

In N_1_4_20, the damage process is different from previous ones. Obtained from the model and illustrated in the left figure of Fig. 3(c), delamination propagation occurs first and develops towards side edge, accompanied with increasing level of concentrated stresses. However, as the 4-laminae sublaminate delaminates from its substrate to a certain degree, fibre compressive failure takes place within the 0° lamina at the location aligned with the delamination front. From that point on, the 4-laminae sublaminate loses much of its stiffness such that at the given level of deformation it would not be stiff enough to generate sufficient amount of energy release rate for the delamination to propagate further. Effectively, the laminate loses the contribution from this sublaminate. The subsequent compressive failure in the 20-laminae core is a natural consequence as it is left to sustain the compression primarily. The dominant damage mechanism is in-plane failure in the 20-laminae sublaminate. The extension of delamination to the full width as shown in the right figure of Fig. 3(c) is not genuine delamination propagation. In fact, it is because of the failure of the neighbouring 0° lamina to which the cohesive elements are attached.

Due to the limited length, the results from remaining models are illustrated in Fig. 3(d)-(f) and only discussed partially. It can be concluded that no significant delamination propagation observed when initial fibre compression failure occurs. At maximum compression load, basically only interface next to 0° laminae fails. This failure is due to severe deformation of the crushed 0° laminae rather than commonly referred "delaminating propagation".

Figure 3. Section view of damage states at initial fibre compression failure and maximum load.

3.2 Relationship between in-plane failure and delamination propagation

In order to illustrate relationship between in-plane failure and delamination propagation, a set of cohesive elements representing the delamination front of the specified initial delamination

is extracted (Fig. 2). As these elements are situated around the model centre, the cosine of the angular position of each element defines its unique location. A contour plot is employed to illustrate the failure process of this element set with the increasing load (Fig. 4). The failure parameter (actually it is the ratio of energy release rate to the critical energy release rate) varies from 0 to 1, where 0 represents the undamaged element and 1 for complete damage. A circle is employed to mark the initial fibre compressive failure. With this kind of contour plots, we can easily observe that, for Model N_1_4_20 (Fig. 4(a)), delamination propagation occurs prior to fibre compression failure as concluded above. However, the phenomenon that fibre compression failure occurs obviously before delamination propagation has not been observed from all remaining models (for example, that in Fig. 4(b), where the contour of the interface between 4th and 5th laminae in Model N_5 shows as a representative case). This is because once stress concentration appears at the delamination front, the tendency of relative movement at the front becomes more severe, which inevitably increases the energy release rate of the cohesive element at the front. Therefore it can be concluded that delamination propagation can occur before in-plane failure. However, in return, in-plane failure is always accompanied with interface failure. It is difficult to distinguish the interface failure due to crushed neighbouring laminae or delamination propagation. Nevertheless, once in-plane failure occurs, it will remain as the dominant damage mechanism and lead to catastrophic failure.

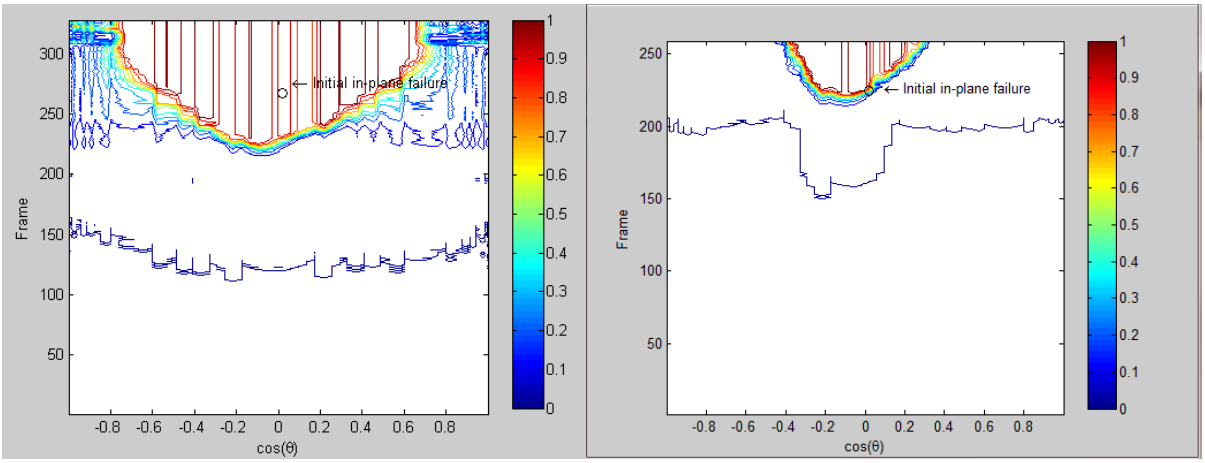

(a) (b)

Figure 4. Damage parameter contour of the cohesive elements at initial delamination front. Curve with corresponding colour valued in spectrum represents certain damage state from no damage (value 0) to complete damage (value 1). Curves once transform to straight line and stretch till figure's top edge representing complete damage of corresponding cohesive element from the time represented by the y-axis' value of the head of the straight line on. (a) The interface between 4th and 5th lamina in Model N_1_4_20, (b) The interface between 4th and 5th lamina in Model N_5.

4. Conclusion

The damage mechanism of CAI is numerically analyzed. It is found that delamination propagation may occur when model with fewer delaminations, the in-plane failure is basically the dominant damage mechanism for model bearing multiple delaminations which is more like the real impacted case. As delamination is generated almost between any two neighbouring laminae due to low speed impact, it is reasonable to predict the residual compression strength only considering in-plane failure mode.

5 Acknowledgement

The first author wishes to acknowledge the PhD studentship offered by AVIC, China.

References

[1] R. Craven, L. Iannucci and R. Olsson. Delamination buckling A finite element study with realistic delamination shapes multiple delaminations and fibre fracture cracks. *Composites: Part A*, 41(2010):684-692, 2010.

[2] H. Chai. One dimensional modeling of failure in laminated plates by delamination buckling. *International journal of solids structures*, 17(11), 1069-1083, 1981.

[3] J. Whitcomb. Strain-energy release rate analysis of plates with postbuckled delaminations. *Journal of composite materials*, 23, 714-734, 1989.

[4] D. Shu and Y. Mai. Buckling of delaminated composites re-examined. *Composite science and technology*, 47(1993), 35-41, 1993.

[5] J. Klug. Efficient modeling of postbuckling delamination growth in composite laminates using plate elements. *AIAA Journal*, 34(1), 178-184, 1996.

[6] H. Ovesy. Post-buckling analysis of composite plates containing embedded delaminations with arbitrary shape by using higher order shear deformation theory. *Composite structures*, 94(2012), 1243-1249, 2012.

[7] M. Moura. Prediction of compressive strength of carbon–epoxy laminates containing delamination by using a mixed-mode damage model. *composite structures*, 50(2000), 151-157, 2000.

[8] J. Whitcomb. Three-dimensional analysis of a postbuckled embedded delamination. *Journal of composite materials*, 23, 862-889, 1989.

[9] H. Chen. Residual compressive strength of laminated plates with delamination. *composite structures*, 47, 711-717.

[10] H. Suemasu. Compressive behavior of impact damaged composite laminates. *16th Int. Conf. on Composite Materials*, Kyoto, Japan, 13 July 2007, 2007.

[11] R. Krueger. An Approach to Assess Delamination Propagation Simulation Capabilities in Commercial Finite Element Codes. NASA. 2008

[12] A. Orifici. Benchmark assessment of automated delamination propagation capabilities in finite element codes for static loading. *Finite Elements in Analysis and Design*, 54, 28-36, 2012

[13] H. Suemasu. A numerical study on compressive behavior of composite plates with multiple. *Composites Science and Technology*, 68, 2562-2567, 2008.

[14] E. Dost. Effect of stacking sequence on impact damage resistance and residual strength for quasi-isotropic laminates. *American society for testing and materials.* Philadelphia, 1991.

[15] P. Chen. A New Method for Compression After Impact Strength Prediction of Composite Laminates. *Journal of composite materials*, 36, 589-610, 2002.

[16] Y. Xiong. A prediction method for the compressive strength of impact damaged composite laminates. *Composite structures*, 30, 357-367, 1995.

[17] X. Tang. *Theory manual of CDTAC 1.0.* Aircraft Strength Research Institute, Xi'an. 1998.

[18] A. Kaddour. Input data for test cases used in benchmarking triaxial failure theories of composites. *Journal of composite materials*, 46(19-20), 2295-2312, 2012.

[19] ASTM D-7137. Standard Test Method for Compressive Residual Strength Properties of Damaged Polymer Matrix Composite Plates. *American Society for Testing and Materials.* 2012.

[20] S. Li. On the symmetry conditions for laminated fibre-reinforced composite structures. *International journal of solids structures*, 29(23), 2867-2880, 1992.